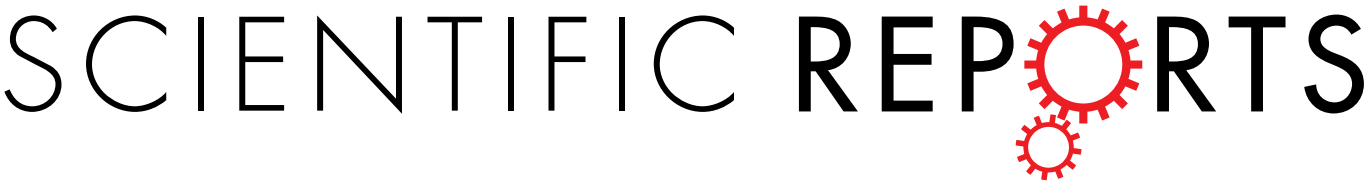

OPEN

Molecular Structure and Dynamics of Water on Pristine and Strained Phosphorene: Wetting and Diffusion at Nanoscale

Received: 08 April 2016
Accepted: 08 November 2016
Published: 06 December 2016

Wei Zhang[1,2,*], Chao Ye[1,*], Linbi Hong[3], Zaixing Yang[4] & Ruhong Zhou[1,3,5]

Phosphorene, a newly fabricated two-dimensional (2D) nanomaterial, has emerged as a promising material for biomedical applications with great potential. Nonetheless, understanding the wetting and diffusive properties of bio-fluids on phosphorene which are of fundamental importance to these applications remains elusive. In this work, using molecular dynamics (MD) simulations, we investigated the structural and dynamic properties of water on both pristine and strained phosphorene. Our simulations indicate that the diffusion of water molecules on the phosphorene surface is anisotropic, with strain-enhanced diffusion clearly present, which arises from strain-induced smoothing of the energy landscape. The contact angle of water droplet on phosphorene exhibits a non-monotonic variation with the transverse strain. The structure of water on transverse stretched phosphorene is demonstrated to be different from that on longitudinal stretched phosphorene. Moreover, the contact angle of water on strained phosphorene is proportional to the quotient of the longitudinal and transverse diffusion coefficients of the interfacial water. These findings thereby offer helpful insights into the mechanism of the wetting and transport of water at nanoscale, and provide a better foundation for future biomedical applications of phosphorene.

As a newly fabricated 2D nanomaterial composed of phosphorus atoms, phosphorene possesses a direct band gap which makes it a natural semiconducting nanomaterial[1,2]. Because of its unique electrical, optical and mechanical properties, phosphorene can be used in a wide range of biomedical applications with promising potential[3–5]. Notably, using a few layers of phosphorene, researchers have successfully fabricated the field-effect transistor[6,7], which is a desirable device for biodetection and biosensing[8–10]. Simulation and experimental results showed that phosphorene in water is more stable than that in air[11,12]. The good stability of phosphorene in water creates the chances for phosphorene's applications in biological fields. Compared to graphene, phosphorene is more biological-friendly due to its less disruption to proteins[4]. Moreover, as photothermal and photodynamic agents, black phosphorus nanosheets (multiple layers of phosphorene) have exhibited excellent potential in killing cancer cells[5,12]. Naturally, wider applications of this novel nanomaterial do require more extensive studies on its interactions with biomolecules, including the wetting and diffusive properties of bio-fluids on its surface.

The structure and dynamics of interfacial water at various nanomaterial surfaces are of fundamental importance for developing these nanomaterials' potential applications in biomedicine and nanofluidics. The structure of water is perturbed heavily near the surfaces which have the potential to affect water diffusion[13,14] and proteins' adsorption[15]. During recent years, the wetting and diffusive properties of water in contact with two-dimensional (2D) nanomaterials, such as graphene[16–20], boron-nitride sheets[16,21,22], WS_2 and MoS_2[23,24], have attracted great attention. These studies have helped the promotion of potential applications of these 2D nanomaterials in both

[1]Institute of Quantitative Biology and Department of Physics, Zhejiang University, Hangzhou 310027, China. [2]Department of Physics, College of Sciences, China University of Mining and Technology, Xuzhou 221116, China. [3]Computational Biology Center, IBM Thomas J. Watson Research Center, Yorktown Heights, NY 10598, USA. [4]Institute of Quantitative Biology and Medicine, SRMP and RAD-X, Collaborative Innovation Center of Radiation Medicine of Jiangsu Higher Education Institutions, Soochow University, Suzhou 215123, China. [5]Department of Chemistry, Columbia University, NY 10027, USA. *These authors contributed equally to this work. Correspondence and requests for materials should be addressed to W.Z. (email: wzhangph@gmail.com) or R.Z. (email: ruhosngz@us.ibm.com)

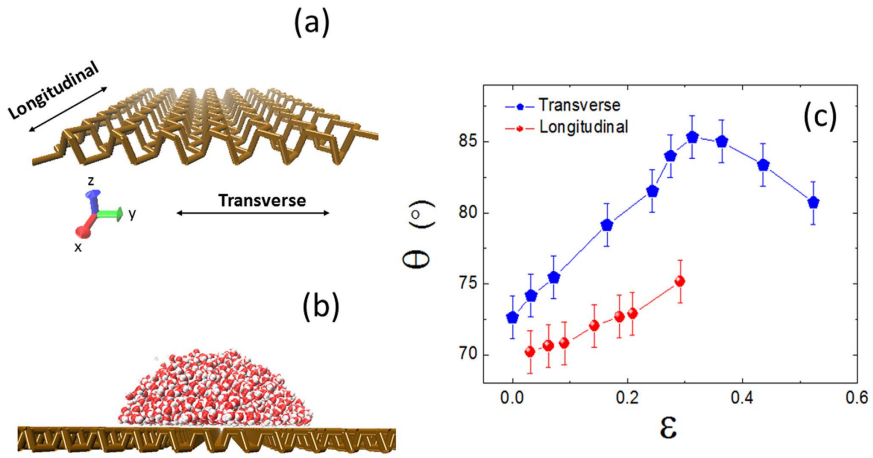

Figure 1. (**a**) Perspective view of transverse and longitudinal directions upon which strains were imposed. **(b)** A snapshot of water droplet on phosphorene ($\varepsilon = 0$; pristine) at the end of the MD simulation. **(c)** The water contact angle θ as a function of the transverse and longitudinal strain.

biomedicine and nanofluidics. However, the structure and dynamics of water on phosphorene, a new member of 2D nanomaterials, are still elusive to the best of our knowledge.

Another promising aspect of phosphorene is its great mechanical flexibility[25], due to the hexagonally arranged phosphorus atoms and the subsequently formed puckered honeycomb structure inside the monolayer of phosphorene. Peng's work demonstrated that phosphorene can withstand a uniaxial tensile strain up to 0.30[26]. Recent computational studies based on the density functional theory (DFT) showed that a single-layer phosphorene could actualize tensile strain (stretching) up to 0.54 while maintaining its original P-P bond and "two-sublayer" (non-planar) structure[27,28]. It has also been demonstrated that all the electrical[29–32], optical[33,34], thermoelectric[35–37] and mechanical[27,30,38] properties of phosphorene could be modified upon mechanical strain. The puckered structure of phosphorene brings anisotropy and negative Poisson's ratio[27,35]. The strain also gives rise to phosphorene's transition between metal and semiconductors[32,35,38]. Therefore, it is of great interest to learn if there is any change in both the structure and dynamics of water on phosphorene upon strain.

In this study, we use molecular dynamics (MD) simulations, which are widely used in the study of the interaction of (bio)molecules with nanomaterials[39–41], to investigate the contact angle, diffusion coefficient, and distribution of water on both pristine and strained phosphorene. We found that the diffusion of water molecules at the surface of phosphorene is anisotropic, and strain-enhanced water diffusion is clearly present. The structure and wetting of water on transverse stretched phosphorene differs from that on the longitudinal stretched one. The contact angle of water droplet non-monotonously changes with imposed transverse strain displaying a parabola-like curve (first increases, then decreases), whereas it increases nearly linearly with imposed longitudinal strain. Also, the distribution of water near the surface of phosphorene exhibits obvious changes when imposed transverse strain increases, while the distribution of water barely changes with the longitudinal strain. Additionally, we found that the contact angle of water on strained phosphorene is proportional to the quotient of the longitudinal and transverse diffusion coefficients of the interfacial water. The dispersion energy and free energy profile of water were further calculated to interpret the above phenomena.

Methods

MD simulations were performed to explore the wetting and diffusive properties of water on both pristine and strained phosphorene. The Gromacs package 4.5.7[42] and OPLS-AA force field[43] were used for the simulations. The SPC/E model was used to model water molecules. Phosphorene with a dimension of 156 Å × 17 Å was chosen for this study. The bond length and bond angle of phosphorene were presented in Fig. S1 in the Supporting Information (SI). The phosphorus atoms were modeled as uncharged Lennard–Jones particles. The depth of potential well ε_{PP}, cross sections σ_{PP} and bond strength constants are set at 0.400 kcal mol^{-1}, 3.33 Å and 297 kcal mol^{-1} Å^2, respectively, following a previous study based on DFT computations and experimental results[44].

Using the umbrella pulling code of Gromacs, we applied a harmonic potential between the centers of mass of two groups of P atoms at two side of phosphorene sheet to produce the strained phosphorene, during which phosphorene was flexible. The strained phosphorene was then fixed throughout the water-phosphorene interaction simulation. Note that the strain being discussed in this study only refers to tensile strain. Phosphorene was therefore stretched along two typical directions: transverse (perpendicular to the pucker) and longitudinal (parallel to the pucker), as shown in Fig. 1(a). Phosphorene with strain $\varepsilon = 0$ corresponds to the pristine phosphorene. Figure S2 in the Supporting Information shows four representative configurations of strained phosphorene. The initial water droplet which was configured as a cubic consisting of 2828 molecules was set onto phosphorene under various strain conditions. During the first few nanoseconds of the simulation, the water droplet gradually converted from a cubic into a hemisphere, as illustrated in Fig. 1(b). We chose 10 morphologies of phosphorene with different degrees of transverse strain, as well as another 10 phosphorene morphologies with different degrees of longitudinal strain for our current study of the interaction with water droplet. Each phosphorene-water system was simulated for 16 ns, and the trajectory of the last 1 ns was extracted for further analysis. Following similar

protocols used in our previous studies[45–51], the particle-mesh Ewald method[52] with a grid spacing of 1.2 Å was applied to simulate the long-range electrostatic interactions, and a typical cutoff of 10 Å was applied for the van der Waals interactions. We increased the z-dimension of the box (a box height of 3 times the slab height) to produce a pseudo-2D Ewald summation. Yeh and Berkowitz's scheme for 2D Ewald summaries is another general method for systems with slab geometry[53]. All simulations were performed in an NVT ensemble at a constant temperature of 298 K by using v-rescale thermostat[54].

The water contact angle θ was measured by fitting the time-averaged liquid-vapor interface[55]. The liquid-vapor interface is defined as the contour with half of the bulk density, while the number density of water droplet was calculated by the time-averaged spatial mesh with a grid spacing of 0.5 Å at a fixed azimuthal angle. The liquid-vapor interface was then fitted into an arc and θ was calculated as the angle of contingence at the liquid-solid interface (refer to Figure S3 in the Supporting Information).

Results and Discussion

The Young's modulus of phosphorene is sensitive to the direction upon which strains were imposed, due to the nanomaterial's anisotropic nature. Figure S4 in Supporting Information illustrates the relationship between the strain at transverse and longitudinal directions and the pull force exerted along these directions. The slope of transverse strain as a function of pull force is clearly steeper than that of longitudinal strain, indicating less stiffness in phosphorene when stretched in the transverse direction. These results are consistent with previous calculations based upon first-principles density functional theory[25,27].

The strains imposed upon phosphorene not only affect its electronic and mechanical properties, but also change the water contact angle on its surface. As shown in Fig. 1(c), the strains exerted in different directions have distinct effects on the water contact angle θ. An increase of the transverse strain ε_T causes θ to first increase, and then to decrease after the peak is reached (parabola-like curve or inverted U-shaped curve). At $\varepsilon_T \sim 0.3$, we observed the maximal contact angle θ_{max}. However, for strains imposed upon the longitudinal direction, the relationship between θ and the longitudinal strain rate ε_L is clearly monotonic (roughly linear). A comparison between the contact angles of water droplet on phosphorene under different directional strains also showed an overall larger contact angles under transverse than longitudinal strain.

The microscopic contact angle has been given by the modified Young's equation. It relates the surface tensions γ of the relevant phase (subscripts S, L, and V for solid, liquid, and vapor phase, respectively), the line tension τ and the droplet base radius r_B (see Fig. S3) with the contact angle θ as[55]:

$$\gamma_{SV} = \gamma_{SL} + \gamma_{LV}\cos\theta + \frac{\tau}{r_B} \quad (1)$$

This equation implies that the contact angle is related to the size of droplet due to line tension. For the sessile water drops with linear shape, it was shown that the wetting depends on the contact line[56]. In this paper, the molecule number of a water droplet on every strained phosphorene is the same (2828 water molecules), but the base radius of the hemispherical water droplet changes with the strain, as shown in Fig. S5. This is one of the reasons why the contact angle of water droplet changes with the strain (Fig. 1c). The Equation 1 can be written as $\cos\theta_\infty = \cos\theta + \tau/\gamma_{LV} r_B$, where θ_∞ is the contact angle for macroscopic droplet. By changing the number of water molecules of droplet (the droplet size), one could derive the macroscopic contact angle θ_∞ of droplet on phosphorene with a certain strain[57] (see ref. 57).

In addition to the droplet size, the contact angle of a water on nanomaterials changes significantly as a function of the water-nanomaterial interaction energy[55]. If one uses a single sheet of LJ atoms in a specific lattice and tunes the interaction energy with the water molecules one would find the initial increase in contact angle due to the higher interaction with the substrate.

Along with the differences in water contact angles, the transverse and longitudinal strains also cause different deformations of the phosphorene surface. While strain in the transverse direction effectively flattens the puckers of phosphorene, longitudinal strain, on the other hand, has little effect on the bending structure of the puckers' ring. This distinct deformation of the phosphorene monolayer leads to different interactions between the water droplet and phosphorene.

The contact angle θ non-monotonically changes with the transverse strain, which is primarily caused by non-monotonic variations of the interaction energy E_{ws}. To analyze the influences of the transverse strain on E_{ws} in detail, we calculated the interaction energy between water droplet and phosphorous atoms in the bottom (E_{ws}^B) and upper (E_{ws}^T) surfaces of the puckered monolayer of phosphorene, respectively (see Fig. 2). Here, $E_{ws} = E_{ws}^B + E_{ws}^T$. With the increase of the transverse strain ε_T, the density of the atoms in the upper surface decreases, thus E_{ws}^T weakens remarkably (Fig. 2, blue curve), resulting in a less favorable interaction and a higher water contact angle. As for the atoms in the bottom surface, they move toward the water droplet (closer to water molecules) which is favorable for the interaction. However, its density decreases at the same time and hence is unfavorable for the interaction. When $\varepsilon_T < \sim 0.16$, the decrease in the density of atoms in the bottom surface dominates the interaction, and E_{ws}^B weakens slightly (see Fig. 2, red curve). When $\varepsilon_T > \sim 0.16$, however, the approach toward the water droplet of the atoms in the bottom surface dominates the interaction, enhancing E_{ws}^B dramatically (Fig. 2, red curve). The combined effect on the interaction from both the upper and bottom surfaces atoms is thus as following, with the increase of ε_T the interaction energy E_{ws} increases firstly and then decreases after ε_T reaches ~0.3, displaying a parabola-like curve as shown in the inset of Fig. 2. On the other hand, as mentioned above, the longitudinal strain has little effect on the bending structure of the pucker ring, thus it displays a monotonic behavior in both the interaction energy with water and the water contact angle (Fig. 1(c)).

In addition to water contact angle, the strain may also affect the structure of water near phosphorene. In order to understand the structure of the interfacial water molecules, we measured the density distribution

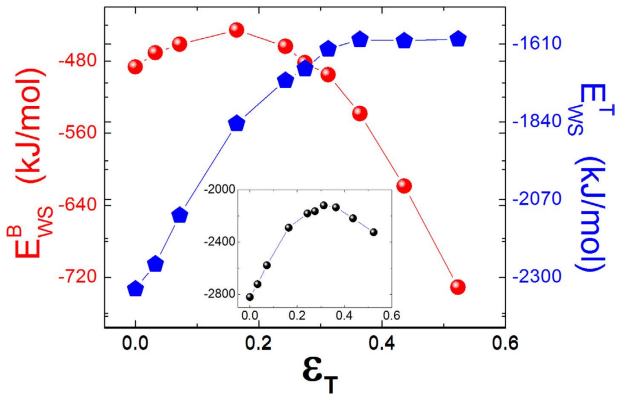

Figure 2. The interaction energy between the water droplet and phosphorous atoms in the bottom (E^B_{ws} red circles) and upper (E^T_{ws} blue pentagons) surfaces of the puckered phosphorene as a function of the strain along the transverse direction. The inset shows the combined interaction energy $E_{ws} = E^B_{ws} + E^T_{ws}$.

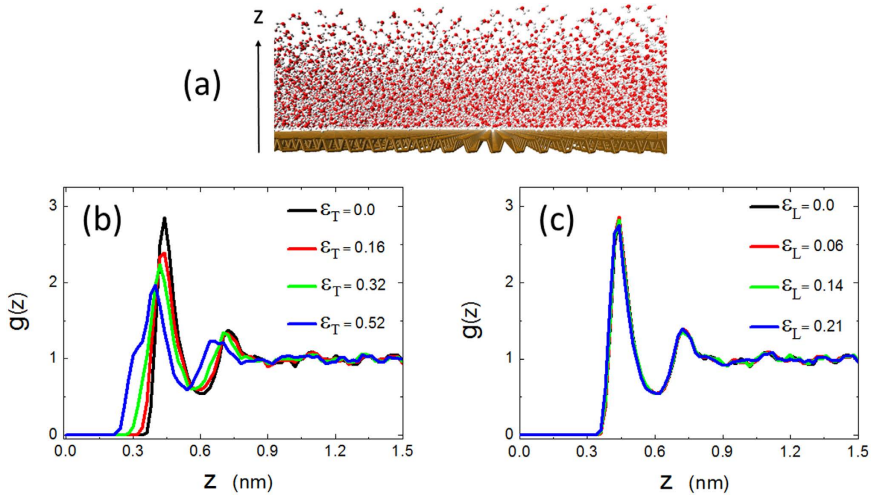

Figure 3. (**a**) A snapshot of the simulation system for studying the density distribution and diffusion of water molecules. **(b)** and **(c)** The density distribution function of oxygen atoms $g(z)$ as a function of the distance z under different magnitudes of strain.

function (DDF) of the oxygen atoms along the direction normal to the surface (z axis). DDF $g(z)$ is defined as in Equation (2):

$$g(z) = \rho(z)/\overline{\rho}. \tag{2}$$

where $\rho(z)$ is the density of oxygen atoms within a thin slice of height z parallel to the surface (the thickness of the slice is set at 0.2 Å), and $\overline{\rho}$ is the mean density of oxygen atoms in the bulk. Note that the zero point of z corresponds to the geometric center of phosphorene in the z-axis direction. A new and much larger thick 2D slab system consisting of 25,662 water molecules, as shown in Fig. 3(a), was used to study the density distribution and diffusion of the water molecules.

Figure 3(b) and (c) show the $g(z)$ of the oxygen atoms near phosphorene under various transverse and longitudinal strains. Due to the dispersive interaction between the phosphorous atoms and water molecules, the structure of water near phosphorene is considerably perturbed from its bulk structure, which displays a double peak character. The double peaks of $g(z)$ in both Fig. 3(b) and (c) indicate the two-layer structure of water in the vicinity of phosphorene, with the first peak corresponding to the first layer of water. The density of the oxygen atoms in the first water layer can be 2.8 times larger than that in the bulk. While $z > \sim 1.0\,nm$, the density fluctuation disappears and the bulk density is recovered. Meanwhile, the difference between Fig. 3(b) and (c) is worth noting. In Fig. 3(b), as the transverse strain increases, both the critical position z_c where oxygen atoms appear and the maximal DDF g_{max} decrease, but the half-width of the first peak W increases (see Table 1). As for the longitudinal strain, it showed almost no effect on $g(z)$, as shown in Fig. 3(c).

The above results demonstrated that the effects of transverse and longitudinal strains on the static structure of interfacial water are distinct, which can be partly attributed to the anisotropic mechanical properties of phosphorene. In the following discussion, we present the effects of the strain on the dynamic properties of interfacial

ε_T	z_c (nm)	g_{max}	W (nm)
0	0.36	2.85	0.08
0.03	0.35	2.68	0.10
0.07	0.34	2.64	0.10
0.16	0.32	2.38	0.10
0.24	0.30	2.26	0.12
0.28	0.30	2.21	0.12
0.31	0.28	2.24	0.12
0.36	0.25	2.14	0.14
0.43	0.24	2.08	0.15
0.52	0.22	1.97	0.18

Table 1. The critical position z_C, the height g_{max} and half-width W of the first peak of the density distribution function (DDF) of oxygen atoms corresponding to various values of the transverse strain ε_T.

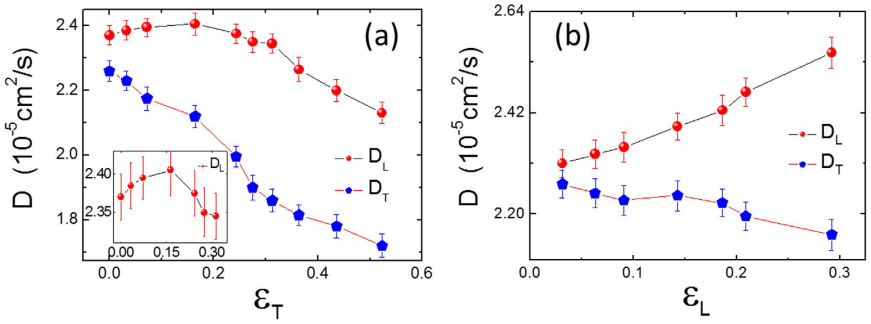

Figure 4. The diffusion coefficient D of water molecules in the first layer as a function of **(a)** the transverse and **(b)** longitudinal strain.

water. To illustrate the dynamical properties clearly, we denote z_m and z_v as the z position of the first peak and valley of DDF, respectively.

In order to examine the dynamic properties of liquid on phosphorene, we begin with the self-diffusion of water molecules in the first layer. The mean squared displacement (MSD) was measured according to the following equation:

$$\langle \Delta \boldsymbol{r}^2(\tau) \rangle = \frac{\sum_{i=1}^{N} \Theta_i(0) \cdot \left\langle |\boldsymbol{r}_i(t+\tau) - \boldsymbol{r}_i(t)|^2 \Theta_i(t) \cdot \prod_{t'=t}^{t+\tau} \Theta_i(t') \right\rangle_t}{\sum_{i=1}^{N} \Theta_i(0) \cdot \left\langle \Theta_i(t) \cdot \prod_{t'=t}^{t+\tau} \Theta_i(t') \right\rangle_t}, \quad (3)$$

where $r_i(t)$ is the position of oxygen atoms of the i th water molecule at time t; τ is the lag time and N is the number of molecules included in this calculation. The angle brackets $<\ldots>_t$ indicate the average over the time t. The function of $\Theta_i(t)$ is 1 if the water molecule i belongs to the first layer at time t and is otherwise 0. MSD in Eq. 3 was evaluated only for the survived water molecule in the first layer (the position of the oxygen atom of water in the region $z_c < z < z_v$). Water molecule in the first layer calculated in original time would jump out from this layer, and the continuous survival probability (CSP)[58] decreases with the duration time (Fig. S6 in SI). The life-time of water in the first layer decreases with the transverse strain in the range (0.00–0.36). Because in this range the interaction energies between water molecules and strained phosphorene decreases with the strain.

The transverse and longitudinal mean squared displacement ($MSD_T = \langle \Delta x^2(\tau) \rangle$ and $MSD_L = \langle \Delta y^2(\tau) \rangle$ respectively) increases linearly with the time interval τ, as shown in Fig. S7. The transverse and longitudinal self-diffusion coefficients, D_T and D_L, are derived from the following equations: $\langle \Delta x^2(\tau) \rangle = 2D_T\tau$ and $\langle \Delta y^2(\tau) \rangle = 2D_T\tau$.

Figure 4 shows the transverse and longitudinal diffusion coefficients of water molecules in the first layer with various strain conditions. It is clear from the separation of the curves as shown in Fig. 4, that the diffusion of water molecules on pristine phosphorene is anisotropic, mainly due to the puckering surface morphology of phosphorene. Compared to motions in the transverse direction, a higher D_L coefficient indicates that it is much easier for water molecules to move along the longitudinal direction. The transverse diffusion coefficient D_T decreases monotonically with increased transverse strain ε_T. The longitudinal diffusion coefficient D_L increases while ε_T is smaller than 0.16, and decreases after ε_T rises above 0.16, as shown in Fig. 4(a) and its inset (again, parabola-like curve or inverted U-shaped curve). The effects of longitudinal strain on the diffusion of interfacial water differ from that of transverse strain. Here, as the longitudinal strain ε_L increases, D_L also increases but D_T decreases. As shown in Fig. 4(b), D_L increases from 2.37 to 2.61 (10^{-5} cm^2/s) in the measured range of ε_L. In contrast, the change

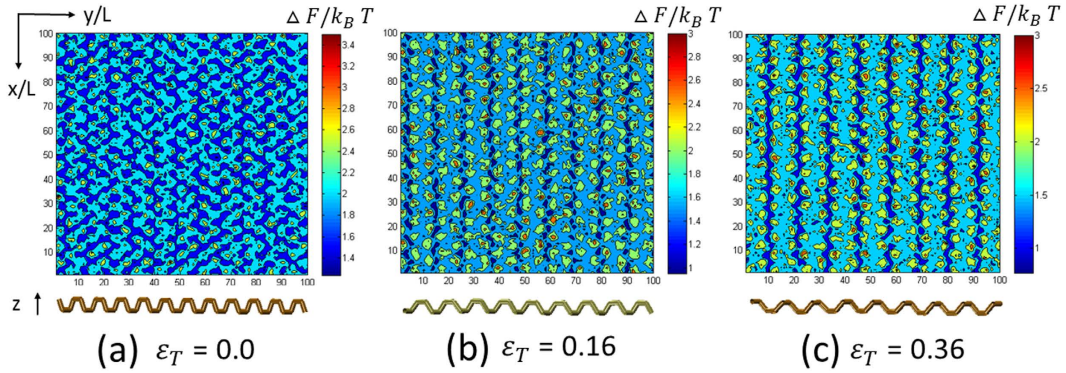

Figure 5. Free energy profile of water within the first layer $\Delta F(x, y)$ scaled by k_BT for three values of ε_T. Here, the scaling parameter L = 0.05 nm.

of D_T is not as significant. Clearly, the effects of ε_T and ε_L on the diffusion of interfacial water are complicated, and all of an anisotropic manner.

To rationalize the diffusion behaviors of the interfacial water, we computed the free energy profile $\Delta F(x, y)$ of water within the first layer ($z_c < z < z_v$) (with a bin width of 5 nm in x and y-directions at the center of phosphorene sheet) with the equation:

$$\Delta F(x, y) = -k_B T \ln P_o(x, y) \tag{4}$$

Here, $P_o(x, y)$ is the spatial probability distribution function of the oxygen atoms of water within the first layer at coordinate (x, y). This approach has been previously applied to examine the friction of water on graphene and boron nitride[22], as well as the free energy landscape of protein folding[59–61]. In Fig. 5, we present $\Delta F(x, y)$ as scaled by k_BT under different transverse strains. The free energy profile $\Delta F(x, y)$ obviously exhibits a "grooved morphology", mimicking the phosphorene surface, which is a clear indication of anisotropy. The minimal free energy regions appear in the grooves of phosphorene. The variation of the free energy profile with the strain arises from the change of the structure of phosphorene. The hopping mechanism of interfacial water would depend upon free energy barrier. A smooth free energy profile is beneficial to the diffusion of the interfacial water. The smoother the free energy profile is (corresponding to smaller energy barrier), the larger the diffusion coefficient of interfacial water becomes.

For the pristine phosphorene ($\varepsilon_T = 0$ and $\varepsilon_L = 0$), the free energy profile $\Delta F(x, y)$ shows clear "zigzag" patterns in the grooved region (see Fig. 5(a)), similar to the so-called "swallow gird". The maximal energy barrier for water molecules to translate along the longitudinal direction is about $1.5\,k_BT$, while it is ~$1.7\,k_BT$ to move in the transverse direction. Thus, it is more difficult for interfacial water molecules to move in the transverse than in the longitudinal direction. As a result, the diffusion coefficient of interfacial water along the longitudinal direction is larger than that along the transverse direction.

Rationalizing the effects of the transverse strain ε_T on the transverse diffusion coefficient D_T. The strain ε_T acts to broaden the interval of free energy ribbons (low-energy region along the groove) which corresponds to the groove width of phosphorene. The broadening of free energy ribbon interval constrains the diffusion of water molecules along the transverse direction, since it introduces more difficulty in water molecules' crossing of broadened energy barrier. Meanwhile, the strain ε_T increases the mean energy barrier for water molecules to move in the transverse direction, thus hindering the motion of water molecules along the transverse direction. Consequently, the transverse diffusion coefficient D_T decreases as ε_T increases, as shown in Fig. 4(a).

Rationalizing the effects of the transverse strain ε_T on the longitudinal diffusion coefficient D_T. With the increase of strain ε_T, the "zigzag" pattern gradually disappears in general and the free energy ribbons becomes smooth in the longitudinal direction (the low-energy region inter-connects, see Fig. 5(b) and (c)), which is favorable for water molecules to diffuse in the longitudinal direction. Thus, the longitudinal diffusion coefficient D_L increases with the increase of ε_T, up to 0.16, as shown in the inset of Fig. 4(a). With further increase of ε_T to be larger than 0.16, the influence of phosphorus atoms at the bottom layer of the groove begins to dominate as mentioned above, which affects water's diffusion as well. As ε_T increases above 0.16, D_L decreases, because of the increased attraction from phosphorus atoms at the bottom of the groove (see Fig. 2).

Rationalizing the effects of the longitudinal strain ε_T on the longitudinal and transverse diffusion coefficients. When phosphorene is under longitudinal strain, the variations of the free energy profile $\Delta F(x, y)$ is different from those under transverse strain (see Fig. S8 in Supporting Information). The longitudinal strain ε_L obviously attenuates the "zigzag" pattern of the free energy ribbon, which accounts for the enhancement of D_L as ε_L increases. However, unlike the effect of ε_T, the longitudinal strain ε_L only narrows the groove width, while shows little effect on its depth. In other words, it increases the mean height of energy barrier (see Fig. S9) but decreases its width. The increased energy barrier constrains the diffusion of water molecules along the transverse direction. On the other hand, the decrease of the width of energy barrier is in favor of water diffusion, thus an

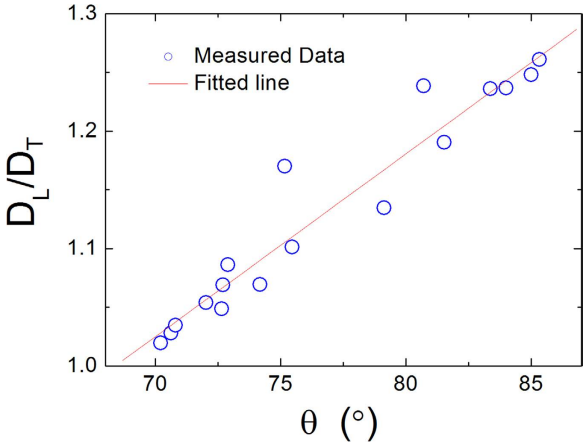

Figure 6. The quotient of D_L/D_T as a function of the contact angle θ of water droplets. The fitting line has the form: $D_L/D_T = \theta \cdot 0.016(^0)^{-1} - 0.06$.

increased D_T. Under the combined influences of these two factors (the increased height and decreased width of energy barrier), as ε_L increases, the transverse diffusion coefficient D_T decreases slightly.

Though the longitudinal strain ε_L obviously smoothes the free energy ribbon and increases the longitudinal diffusion coefficient of interfacial water, it has almost no effects on the density distribution function (DDF) $g(z)$ (see Fig. 3(c)). The DDF $g(z)$, however, obviously changes with the transverse strain ε_T (Fig. 3(b)), which is caused by the flattening of the puckered surface of phosphorene. The flattening of the surface of phosphorene leads to the decrease of the critical position z_c. The increase of the half-width W and the decrease of the height g_{max} are related to the energy profile of single water molecule on phosphorene surface as a function of distance from surface (see Fig. S10). As shown in Fig. S10, energy profile curve are similar to LJ potential and has a minimum value. With the increase of the transverse strain, the minimum energy value and the half-width of the energy valley increase. Consequently, DDF $g(z)$ is related not only to the dispersion energy between water and phosphorene, but also to the distribution of water molecules on phosphorene's surface.

Interestingly, the quotient D_L/D_T, instead of D_L or D_T alone, exhibits a roughly linear relationship with the contact angle θ of water droplet, as shown in Fig. 6. The variation of the width and depth of the groove of phosphorene caused by the strain directly affects the interaction energy E_{ws} and the free energy profile $\Delta F(x, y)$. The contact angle θ and the diffusion coefficient of water molecules in the first layer, on the other hand, are mainly determined by the interaction energy E_{ws} and free energy profile $\Delta F(x, y)$. The free energy profile $\Delta F(x, y)$ jointly affects the transverse and longitudinal diffusion of water molecules. In this sense, the contact angle θ should be related to the diffusion of water molecules along transverse and longitudinal directions. However at present, we have not yet found a quantitative interpretation regarding the relationship between the ratio D_L/D_T and water contact angle θ, which needs further investigation and experimental validation.

Changing the pattern of the puckering surface of phosphorene by the strain could effectively enhance or attenuate the diffusion of interfacial water molecules, which might provide insight for controlling/designing the motion of interfacial molecules. By controlling the strain, one could construct continuous diffusion (or wetting) gradient, which is of interest in artificial microscopic walk[62,63]. The anisotropic diffusion of water molecules near phosphorene surface may also affect phosphorene's motion in complex biological systems, which is of importance for phosphorene's potential biomedical applications, such as localized bioprobes and drug delivery.

Conclusions

In this study, we investigated the wetting and diffusive properties of water near both pristine and strained phosphorene with MD simulations. It was found that the pristine phosphorene is of weak hydrophobicity, with a water contact angle of ~72°. As for the interactions between water droplet and phosphorene under different strains (stretchings), we discovered that the water contact angle θ displays a parabola-like curve with the transverse strain (first increases, then decreases, as the transverse strain reaches a critical threshold of 0.3). However, for the longitudinal strain, the contact angle θ increases monotonically as the strain increases. The changes in water contact angle are mainly determined by the interaction energy between the water droplet and phosphorene. The structure of the interfacial water dramatically changes with the transverse strain ε_T, but the longitudinal strain ε_L has almost no effect on water's structure.

While the diffusion of water molecules near pristine phosphorene surface is anisotropic, the longitudinal diffusion coefficient D_L is larger than that (D_T) in the transverse direction. As the transverse strain ε_T increases, D_T decreases monotonically, while D_L exhibits a parabola-like curve (or inverted U-shaped curve). The longitudinal strain ε_L, on the other hand, causes D_L to increase, and D_T to decrease monotonically. We also calculated the free energy profile $\Delta F(x, y)$ to determine the main cause of variations in the diffusion of water molecules near phosphorene. It was shown that the smoothing of the energy landscape enhances D_L, and the increased energy barrier causes D_T to decrease. Last but not least, we found that interestingly the quotient D_L/D_T is positively correlated with the contact angle θ.

As a novel 2D nanomaterial, phosphorene has the potential to be widely used in biomedical applications in the near future. Therefore it is necessary to investigate their interactions with various bio-fluids, including the wetting and diffusive properties of water on both pristine and strained phosphorene. Our study should help with understanding and manipulating the wetting and diffusive properties of liquid on phosphorene, which is critical for phosphorene's application in the fields of biomedicine and nanofluidics.

References

1. Lu, W. *et al.* Plasma-assisted fabrication of monolayer phosphorene and its Raman characterization. *Nano Research* **7,** 853–859 (2014).
2. Liu, H., Du, Y., Deng, Y. & Ye, P. D. Semiconducting black phosphorus: synthesis, transport properties and electronic applications. *Chem. Soc. Rev.* **44,** 2732–2743 (2015).
3. Ling, X., Wang, H., Huang, S., Xia, F. & Dresselhaus, M. S. The renaissance of black phosphorus. *Proceedings of the National Academy of Sciences of the United States of America* **112,** 4523–4530 (2015).
4. Zhang, W. *et al.* Revealing the importance of surface morphology of nanomaterials to biological responses: Adsorption of the villin headpiece onto graphene and phosphorene. *Carbon* **94,** 895–902 (2015).
5. Sun, Z. *et al.* Ultrasmall Black Phosphorus Quantum Dots: Synthesis and Use as Photothermal Agents. *Angewandte Chemie* **54,** 11526–11530 (2015).
6. Li, L. *et al.* Black phosphorus field-effect transistors. *Narure nanotechnology* **9,** 372–377 (2014).
7. Liu, H. *et al.* Phosphorene: An Unexplored 2D Semiconductor with a High Hole Mobility. *ACS Nano* **8,** 4033–4041 (2014).
8. Im, H., Huang, X. J., Gu, B. & Choi, Y. K. A dielectric-modulated field-effect transistor for biosensing. *Nature nanotechnology* **2,** 430–434 (2007).
9. Martinez, M. T. *et al.* Label-Free DNA Biosensors Based on Functionalized Carbon Nanotube Field Effect Transistors. *Nano letters* **9,** 530–536 (2009).
10. Tian, B. *et al.* Three-dimensional, flexible nanoscale field-effect transistors as localized bioprobes. *Science* **329,** 830–834 (2010).
11. Wang, G., Slough, W. J., Pandey, R. & Karna, S. P. Theoretical Study of Stability of Phosphorene in Air. *arXiv:*1508.07461v1 (2015).
12. Wang, H. *et al.* Ultrathin Black Phosphorus Nanosheets for Efficient Singlet Oxygen Generation. *Journal of the American Chemical Society* **137,** 11376–11382 (2015).
13. Kim, J. S. *et al.* Between scylla and charybdis: hydrophobic graphene-guided water diffusion on hydrophilic substrates. *Sci Rep* **3,** 2309 (2013).
14. Li, Q., Song, J., Besenbacher, F. & Dong, M. Two-dimensional material confined water. *Accounts of chemical research* **48,** 119–127 (2015).
15. Peter, E. K., Agarwal, M., Kim, B., Pivkin, I. V. & Shea, J. E. How water layers on graphene affect folding and adsorption of TrpZip2. *The Journal of chemical physics* **141,** 22D511 (2014).
16. Li, H. & Zeng, X. Wetting and Interfacial Properties of Water Nanodroplets in Contact with Graphene and Monolayer Boron-Nitride Sheets. *ACS Nano* **6,** 2401–2409 (2012).
17. Taherian, F., Marcon, V., van der Vegt, N. F. & Leroy, F. What is the contact angle of water on graphene? *Langmuir: the ACS journal of surfaces and colloids* **29,** 1457–1465 (2013).
18. Li, X., Li, L., Wang, Y., Li, H. & Bian, X. Wetting and Interfacial Properties of Water on the Defective Graphene. *The Journal of Physical Chemistry C* **117,** 14106–14112 (2013).
19. Wei, N., Lv, C. & Xu, Z. Wetting of graphene oxide: a molecular dynamics study. *Langmuir: the ACS journal of surfaces and colloids* **30,** 3572–3578 (2014).
20. Chen, Z., Dong, L., Yang, D. & Lu, H. Superhydrophobic graphene-based materials: surface construction and functional applications. *Advanced materials* **25,** 5352–5359 (2013).
21. Gordillo, M. C. & Marti, J. Wetting and prewetting of water on top of a single sheet of hexagonal boron nitride. *Phys Rev E* **84** (2011).
22. Tocci, G., Joly, L. & Michaelides, A. Friction of water on graphene and hexagonal boron nitride from ab initio methods: very different slippage despite very similar interface structures. *Nano letters* **14,** 6872–6877 (2014).
23. Chow, P. K. *et al.* Wetting of Mono and Few-Layered WS2 and MoS2 Films Supported on SiSiO2 Substrates. *ACS Nano* **9,** 3023–3031 (2015).
24. Kozbial, A., Gong, X., Liu, H. T. & Li, L. Understanding the Intrinsic Water Wettability of Molybdenum Disulfide (MoS2). *Langmuir: the ACS journal of surfaces and colloids* **31,** 8429–8435 (2015).
25. Wei, Q. & Peng, X. Superior mechanical flexibility of phosphorene and few-layer black phosphorus. *Appl Phys Lett* **104,** 251915 (2014).
26. Peng, X., Copple, A. & Wei, Q. Strain engineered direct-indirect band gap transition and its mechanism in 2D phosphorene. arxiv. org/pdf/1403.3771 (2014).
27. Jiang, J. W. & Park, H. S. Negative poisson's ratio in single-layer black phosphorus. *Nat Commun* **5** (2014).
28. Hu, T. & Dong, J. Structural phase transitions of phosphorene induced by applied strains. *Physical Review B* **92** (2015).
29. Fei, R. & Yang, L. Strain-engineering the anisotropic electrical conductance of few-layer black phosphorus. *Nano letters* **14,** 2884–2889 (2014).
30. Hu, T., Han, Y. & Dong, J. Mechanical and electronic properties of monolayer and bilayer phosphorene under uniaxial and isotropic strains. *Nanotechnology* **25,** 455703 (2014).
31. Ge, Y., Wan, W., Yang, F. & Yao, Y. The strain effect on superconductivity in phosphorene: a first-principles prediction. *New Journal of Physics* **17,** 035008 (2015).
32. Li, Y., Yang, S. & Li, J. Modulation of the electronic properties of ultrathin black phosphorus by strain and electrical field. *The Journal of Physical Chemistry C* **118,** 23970−23976 (2014).
33. Çakır, D., Sahin, H. & Peeters, F. M. Tuning of the electronic and optical properties of single-layer black phosphorus by strain. *Physical Review B* **90** (2014).
34. Mehboudi, M. *et al.* Strain and the optoelectronic properties of nonplanar phosphorene monolayers. *Proceedings of the National Academy of Sciences of the United States of America* **112,** 5888–5892 (2015).
35. Qin, G. *et al.* Hinge-like structure induced unusual properties of black phosphorus and new strategies to improve the thermoelectric performance. *Sci Rep* **4,** 6946 (2014).
36. Lv, H. Y., Lu, W. J., Shao, D. F. & Sun, Y. P. Enhanced thermoelectric performance of phosphorene by strain-induced band convergence. *Physical Review B* **90** (2014).
37. Konabe, S. & Yamamoto, T. Significant enhancement of the thermoelectric performance of phosphorene through the application of tensile strain. *Applied Physics Express* **8,** 015202 (2015).
38. Elahi, M., Khaliji, K., Tabatabaei, S. M., Pourfath, M. & Asgari, R. Modulation of electronic and mechanical properties of phosphorene through strain. *Physical Review B* **91** (2015).
39. Zhou, R. Modeling of Nanotoxicity: Molecular Interactions of Nanomaterials with Bionanomachines. (Springer, New York; 2015).
40. Ge, C. *et al.* Binding of blood proteins to carbon nanotubes reduces cytotoxicity. *Proc. Natl. Acad. Sci. USA* **108,** 16968–16973 (2011).

41. Tu, Y. *et al.* Destructive extraction of phospholipids from Escherichia coli membranes by graphene nanosheets. *Nat Nanotechnol* **8,** 594–601 (2013).
42. Pronk, S. *et al.* GROMACS 4.5: a high-throughput and highly parallel open source molecular simulation toolkit. *Bioinformatics* **29,** 845–854 (2013).
43. Jorgensen, W. L., Maxwell, D. S. & Tirado-Rives, J. Development and testing of the OPLS all-atom force field on conformational energetics and properties of organic liquids. *Journal of the American Chemical Society* **118,** 11225–11236 (1996).
44. Ballone, P. & Jones, R. O. A reactive force field simulation of liquid-liquid phase transitions in phosphorus. *The Journal of chemical physics* **121,** 8147–8157 (2004).
45. Liu, P., Huang, X., Zhou, R. & Berne, B. J. Observation of a dewetting transition in the collapse of the melittin tetramer. *Nature* **437,** 159–162 (2005).
46. Zhou, R., Huang, X., Margulis, C. J. & Berne, B. J. Hydrophobic collapse in multidomain protein folding. *Science* **305,** 1605–1609 (2004).
47. Fitch, B. G. *et al. Blue Matter: Strong scaling of molecular dynamics on Blue Gene/L*. (Springer Berlin Heidelberg, 2006).
48. Das, P., King, J. A. & Zhou, R. Aggregation of gamma-crystallins associated with human cataracts via domain swapping at the C-terminal beta-strands. *Proc. Natl. Acad. Sci. USA* **108,** 10514–10519 (2011).
49. Das, P. & Zhou, R. Urea-induced drying of carbon nanotubes suggests existence of a dry globule-like transient state during chemical denaturation of proteins. *J. Phys. Chem. B* **114,** 5427–5430 (2010).
50. Li, J. *et al.* Hydration and dewetting near graphite-CH(3) and graphite-COOH plates. *J. Phys. Chem. B* **109,** 13639–13648 (2005).
51. Yang, Z., Wang, Z., Tian, X., Xiu, P. & Zhou, R. Amino acid analogues bind to carbon nanotube via pi-pi interactions: comparison of molecular mechanical and quantum mechanical calculations. *J. Chem. Phys.* **136,** 025103 (2012).
52. Darden, T., York, D. & Pedersen, L. Particle mesh Ewald: An N·log(N) method for Ewald sums in large systems. *The Journal of chemical physics* **98,** 10089 (1993).
53. Yeh, I.-C. & Berkowitz, M. L. Ewald summation for systems with slab geometry. *The Journal of chemical physics* **111,** 3155 (1999).
54. Bussi, G., Donadio, D. & Parrinello, M. Canonical sampling through velocity rescaling. *The Journal of chemical physics* **126,** 014101 (2007).
55. Werder, T., Walther, J. H., Jaffe, R. L., Halicioglu, T. & Koumoutsakos, P. On the Water−Carbon Interaction for Use in Molecular Dynamics Simulations of Graphite and Carbon Nanotubes. *The Journal of Physical Chemistry B* **107,** 1345–1352 (2003).
56. Cheng, D. F. & McCarthy, T. J. Using the fact that wetting is contact line dependent. *Langmuir: the ACS journal of surfaces and colloids* **27,** 3693–3697 (2011).
57. Luan, B. & Zhou, R. Wettability and friction of water on a MoS2 nanosheet. *Appl Phys Lett* **108,** 131601 (2016).
58. Malani, A. & Ayappa, K. G. Relaxation and jump dynamics of water at the mica interface. *The Journal of chemical physics* **136,** 194701 (2012).
59. Zhou, R. Trp-cage: folding free energy landscape in explicit water. *Proc. Natl. Acad. Sci. USA* **100,** 13280–13285 (2003).
60. Zhou, R. & Berne, B. J. Can a continuum solvent model reproduce the free energy landscape of a beta -hairpin folding in water? *Proc. Natl. Acad. Sci. USA* **99,** 12777–12782 (2002).
61. Zhou, R., Berne, B. J. & Germain, R. The free energy landscape for beta hairpin folding in explicit water. *Proc. Natl. Acad. Sci. USA* **98,** 14931–14936 (2001).
62. Wang, T. *et al.* The mechanism for the motion of nanoscale water droplet induced by wetting gradient: A molecular dynamic study. *Computational Materials Science* **105,** 39–46 (2015).
63. Steimel, J. P., Aragones, J. L. & Alexander-Katz, A. Artificial Tribotactic Microscopic Walkers: Walking Based on Friction Gradients. *Physical Review Letters* **113** (2014).

Acknowledgements

We thank Binquan Luan and Bruce Berne for helpful discussions. This research is supported in part by the National Natural Science Foundation of China (Grant Nos 11604381, 11574224, 11374221, and 21320102003), the Natural Science Foundation of Jiangsu Province (Grant No. BK20160238) and China Postdoctoral Science Foundation (Grant Nos 2015T80610 and 2014M560473). A Project Funded by the Priority Academic Program Development of Jiangsu Higher Education Institutions (PAPD), and Jiangsu Provincial Key Laboratory of Radiation Medicine and Protection. R.Z. acknowledges the support from IBM Blue Gene Science Program (W1258591, W1464125, W1464164).

Author Contributions

W.Z. and R.Z. conceived and designed the research. W.Z., L.H., Z.Y. and R.Z. co-wrote the manuscript. W.Z. and C.Y. carried out the molecular dynamics simulations. W.Z. and C.Y. analyzed the data. All authors discussed the results and commented on the manuscript.

Additional Information

Supplementary information accompanies this paper at http://www.nature.com/srep

Competing financial interests: The authors declare no competing financial interests.

How to cite this article: Zhang, W. *et al.* Molecular Structure and Dynamics of Water on Pristine and Strained Phosphorene: Wetting and Diffusion at Nanoscale. *Sci. Rep.* **6**, 38327; doi: 10.1038/srep38327 (2016).

Publisher's note: Springer Nature remains neutral with regard to jurisdictional claims in published maps and institutional affiliations.